Journal of Metals, Materials and Minerals, Vol. 32, No. 3, pp. 32-42, 2022

A molecular dynamics simulation study to investigate the effect of C60 on thermo-mechanical and elastic properties of DGEBA/DETA nanocomposites

Dhritiman TALUKDAR[1], Sudipta HALDER[1,2,3,*], Subhankar DAS[1,4], M. S. GOYAT[5,*], Abhishek Kumar MISHRA[5,*]

[1] *Department of Mechanical Engineering, National Institute of Technology Silchar, Silchar-788010, Assam, India.*
[2] *Alabama Transportation Institute, The University of Alabama, Tuscaloosa, AL 35487, USA*
[3] *Aerospace Engineering and Mechanics, Center for Advanced Vehicle Technologies, The University of Alabama, Tuscaloosa, AL 35487, USA*
[4] *Department of Mechanical Engineering, Siddharth Institute of Engineering and Technology, Puttur, India*
[5] *Department of Physics, Applied Science Cluster, School of Engineering, University of Petroleum & Energy Studies, Dehradun 248007, Uttarakhand, India*

***Corresponding author e-mail:** sudiptomec@gmail.com, goyatmanjeetsingh@gmail.com, akmishra@ddn.upes.ac.in

Received date:
26 February 2022
Revised date
13 June 2022
Accepted date:
3 July 2022

Keywords:
Fullerene;
Molecular dynamics simulation;
Epoxy composites;
Thermomechanical properties;
Mechanical properties

Abstract

Molecular dynamics simulations were performed to investigate the effect of fullerenes (C60) on the thermal and mechanical properties of a cross-linked epoxy system composed of epoxy resin DGEBA and curing agent DETA. Hence, a comparative investigation was performed on the thermal and mechanical properties of DGEBA/DETA reinforced with 2.3 wt% C60 and neat epoxy systems. Properties such as glass transition temperature (GTT), coefficients of thermal expansion (CTE), and elastic properties at different cross-linking densities. Simulation results indicated that the GTT of the epoxy increased by about 25 K due to the presence of C60. The effect of C60 on the CTE was very less, and at higher crosslinking densities, an increase in CTE before the glass transition was observed. It was also observed that the effect of C60 on mechanical properties is dependent on the crosslinking density. The young's modulus of the epoxy/C60 system at a high strain rate showed a drastic decrease as compared to the neat epoxy system at higher crosslinking densities. The highest value of young's modulus of the epoxy/C60 system was observed at 65% crosslinking density.

1. Introduction

Epoxy resin with two or more epoxide groups allows the formation of a 3D-cross-linked structure when reacted with amines, anhydrides, phenols, or thiols. The superior adhesive and mechanical properties like a low creep, high-temperature performance, high modulus, and fracture toughness are results of the 3D-cross-linked structure. Along with this, their lightweight makes them the ideal structural material for various sectors including aerospace, space vehicles, marine vessels, adhesives, and automotive.

Among the wide varieties of epoxy resins like Bisphenol-A, Bisphenol-F, Novolacs, Aliphatic, and Glycidylamine epoxy resins, diglycidyl ether of bisphenol-A (DGEBA) with IUPAC name 2-[[4-[2-[4-(Oxiran-2-ylmethoxy)phenyl]propan-2-yl]phenoxy]methyl] oxirane was chosen in this study because of its high mechanical strength, excellent adhesion, high chemical and corrosion resistance, high heat resistance, dimensional stability properties, and durability in harsh environments [1-4]. Inherently brittle in nature and poor fracture toughness of neat epoxy resin restricts its application in various high-performance structures. Several investigations have been carried out to enhance the fracture toughness by incorporating carbon-based nano-fillers like graphene, CNT and C60 [5-8]. Carbon/epoxy nano-composite materials are one of the vital materials in the modern aircraft industry because of their high specific strength. However, huge time consumption and the expensive nature of experimental investigation impose limitations on them.

Lin and Khare [10] studied cross-linked epoxy-POSS [Polyhedral Oligomeric Silsesquioxane] nanocomposites using molecular dynamics (MD) simulations [9] and found that the incorporation of POSS particles (at 5 wt%) in the cross-linked epoxy resin leads to a weak tendency for lowering the coefficient of volume thermal expansion but does not cause a measurable change in the glass transition temperature [*GTT]*. Frankland and co-researchers [11] investigated the effect of polymer–nanotube crosslinking on critical load transfer mechanism from carbon nanotubes to polymer matrix using MD simulations and found that long-nanotube composites show an increase in the stiffness relative to the polymer. Rahman and Haque [12] investigated mechanical properties of DGEBF-TETA/graphene nano-composite using a fully atomistic model with a Polymer Consistent Force Field, whereas Khare *et al* [13] studied volumetric, structural, and dynamic properties of DGEBA-DDS (diglycidyl ether of bisphenol-A -4,4'-diaminodiphenyl-sulfone)/CNT (carbon nanotube) with the General Amber Force Field using MD simulation. Jiang *et al* [13] used the (Condensed-phase Optimized Molecular Potentials for Atomistic Simulation Studies) COMPASS

force field on an all-atom model of DGEBA-THPA/SWCNT nanocomposite to predict its thermo-mechanical properties across the glass transition. An increase in GTT was indicated from their simulations, resulting due to the incorporation of SWCNTs in the epoxy matrix. Adnan *et al* [14] investigated the effect of the size of C60 on elastic properties of polymer nanocomposites, where significant enhancement of the elastic properties of nanocomposites with the reduction of buckyball size was observed. Ferdous *et al* [15] studied the effects of dispersion of C60 and the intensity of filler and matrix interface attractions on the mechanical properties of polymer nanocomposites. Their simulation results showed that the enhancement in the mechanical properties of nanocomposites is independent of the condition of the interface and solely depends on the extent of an increase in overall matrix density.

A significant amount of literature is already available on experimental and computational studies of CNT and GNP (Graphene nano-platelets) dispersed in the epoxy matrix. However, comparatively fewer computational studies have been conducted on fullerene/epoxy nano-composites. Jeyranpour *et al* [16] reported the effect of fullerene on the thermo-mechanical properties of cross-linked resin epoxy by MD simulations, using a unique resin system Araldite LY 5052/Aradur HY 5052, which is quite different from the ordinary epoxy. They studied the thermal and mechanical properties of the 2 combinations of neat epoxy systems, and 8.64% C60 and 15.9% C60 containing epoxy systems. Their simulation results indicated that the GTT has slightly changed and CTE declined for different concentrations of the filler reinforced epoxy systems. Various mechanical properties including Young's, bulk moduli; shear moduli, Poisson's ratio were also reported and its density was found to be significantly improved in the case of filler reinforced epoxy systems. In another work, Gao *et al* [17] reported the effect of C60 concentration and PB-C60 interaction on the GTT using the united atom model of *cis*-1,4-poly(butadiene) (*cis*-PB). They studied numerous chain dynamics properties like atom translational mobility, bond/segment reorientation dynamics, torsional dynamics, conformational transition rate, and dynamic heterogeneity of the *cis*-PB chains. They reported that the addition of C60 weight fraction because of its inhibition effect on the mobility of the cis-PB chains affects the GTT. Similarly, other reports study the effect of C60 type nanofillers on the thermal and mechanical properties of the epoxy nanocomposites [14,18-20]. We note that in all the reported works filler concentration is different even if the filler is the same, the epoxy matrix type is different. The epoxy systems with different grades such as some containing aliphatic amines based hardeners and some containing aromatic amines based hardeners due to this the monomers of epoxy resin are different as well as the monomers of the hardener are different. The molecular dynamic simulations in such cases make the comparison and analysis of the results quite complex.

In this present study density functional theory (DFT) and MD, simulations have been performed to estimate the material properties of the DGEBA/DETA epoxy system reinforced with 2.3 wt% C60 (which is quite different in terms of studies performed by Jeyranpour *et al* [16] with higher content of C60, additionally, different epoxy systems were used in both the studies*).* The present work is also different from the work carried out by Gao *et al* [17] due to the difference in the type of the polymer matrix as well as the variation in the properties studied such as thermal and thermo-mechanical properties. However, some recent works of Badjian *et al* [21] and Yang *et al* [22] on MD studies on mechanical behaviors and thermal conductivities of carbon nanobud reinforced epoxy composites provides deep insight on the improvement of the properties. But, the present study is different from the reported studies in terms of thermo-mechanical, and elastic properties of C60 reinforced DGEBA/DETA epoxy system such as glass transition temperature (GTT*),* coefficients of thermal expansion (CTE), and Young's modulus at different cross-linking densities and different temperatures. The results were compared with that of the neat epoxy system. However, in future research, results such as surface modification of C60, interface properties between C60 and the epoxy matrix, different buckyball sizes, different volume fractions of the C60 can be considered.

2. Modeling and simulation details

2.1 Atomistic modeling and atomic interactions

Firstly, quantum chemical calculations were realized at the DFT level as implemented in the Gaussian03 program [23] and analyzed with Gauss View [24]. Geometries of the DGEBA and DETA molecules were fully optimized using the 6-31g (d,p) basis set at the DFT level and were mainly carried out in the framework of the Becke-Lee-Yang-Parr [B3LYP] functional [25-28]. DFT optimized geometries of both DGEBA and DETA are presented in Figure 1, with values of optimized bond length in Table S1 and Table S2.

We next present molecular dynamic simulations of two-component epoxy networks. An epoxy resin, consisting of glycidyl ether of bisphenol A ($C_{21}H_{24}O_4$) or DGEBA with two numbers of an epoxy group and having a molecular weight of 340.419 g·mol^{-1} [29] is used in the present simulation. Hardener, diethyl triamine (DETA) with chemical formula $C_4H_{13}N_3$ having three amine groups and molecular weight of 103.167 g·mol^{-1} [29] has been considered as curing agent to prepare the two-component epoxy network.

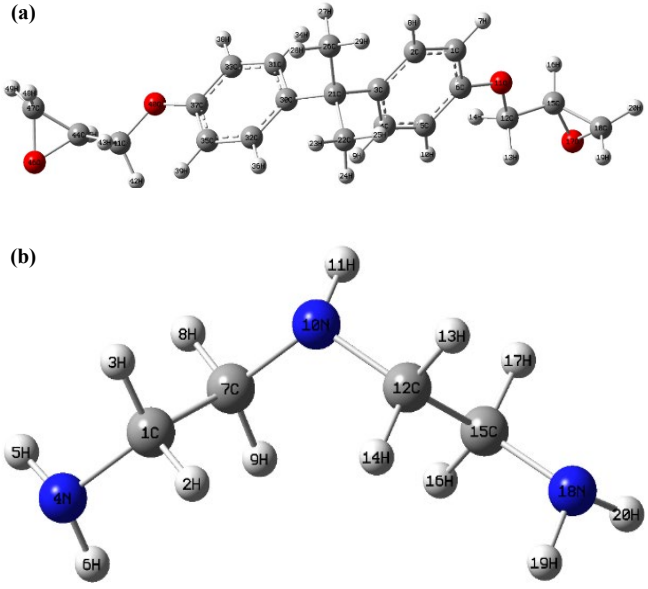

Figure 1. DFT optimize structures of (a) DGEBA, (b) DETA.

The molecular model of epoxy monomer (DGEBA), hardener monomer (DETA), and C60 molecule were prepared using Avogadro [30]. The CHARMM [31] force field is a free parameter set that can be used to describe the atomic interactions in MM (Molecular Mechanics) and MD simulations. It was validated to be an all-purpose force field by Momany and Rone [31]. Apart from being a free force field, it has other advantages like simplicity and expandability to un-parameterized chemical groups. It is mostly used for computational medicinal chemistry research (i.e., drug design) but is also found important for material science. The group behind the program provides optimized parameterizations of a large number of molecules in their CHARMM force field which is a class I force field. CHARMM was developed for macromolecules like proteins and lipids but has, in recent years, also been extended with the CHARMM General Force Field (CGenFF) [32,33], that is, made for smaller organic molecules. The parameterization procedure presented in [33] allows the extension of the force field to chemical groups that are not explicitly covered in the force field. The CGenFF is the force field used for the epoxy molecules in this work, and its potential energy function shown in (1) is a sum of bonded and non-bonded interactions between the atoms in a certain molecule.

$$E(r^n) = E_{bonded} + E_{non\text{-}bonded} \quad (1)$$

The bonded interactions are bonds, angles, dihedrals, impropers, Urey-Bradley and a 2D dihedral energy correction MAP (CMAP). The CMAP is normally used only for modeling backbone peptides and has not been used in this work. This leaves the bonded energy to have four terms as in (2)

$$E_{bonded} = \sum_{bonds} k_b(b\text{-}b_0)^2 + \sum_{angles} k_\theta(\theta\text{-}\theta_0)^2 + \sum_{dihedrals} K_\omega(1 + cos(n\omega\text{-}\delta)) + \sum_{impropers} K_{imp}(\varphi\text{-}\varphi_0)^2 \quad (2)$$

Where k_b, k_θ, K_ω, and K_{imp} are the bond, angle, dihedral angle, and improper dihedral angle force constants, respectively; b, θ, ω and φ are the bond length, bond angle, dihedral angle, and improper torsion angle, respectively, with the subscript zero representing the equilibrium values for the individual terms. (Note that they are not equilibrium values taken from QM calculations). The dihedral term includes $n$and δ which are the dihedral multiplicity and phase shift, respectively. The *bond style harmonic* of the LAMMPS code, which represents the first term of (2) was used for calculating the bond interactions for the epoxy molecules. Similarly, the *angle style harmonic*, *dihedral style charm,* and *improper style harmonic* were used for calculating the second, third, and fourth terms of (2), respectively. The non-bonded energy is the energy associated with Coulomb interactions and vdW forces. The Coulomb interaction originating from partial atomic charges is modeled as the electrostatic energy between point charges while the vdW forces are modeled by a 12-6 Lennard-Jones (LJ) potential with a repulsive term, originating from Pauli repulsion, and an attractive term originating from the vdW dispersion forces between two atom cores. The expression used for taking care of the nonbonded interactions of the epoxy and C60 molecules is presented in equation (3) below

$$E_{non\text{-}bonded} = \sum_{non\text{-}bonded} \left\{ \varepsilon \left[\left(\frac{\sigma_{ij}}{r_{ij}}\right)^{12} - \left(\frac{\sigma_{ij}}{r_{ij}}\right)^{6} \right] + \frac{q_i q_j}{4\pi\varepsilon_1 r_{ij}} \right\} \quad (3)$$

Where r_{ij} is the distance between the interacting atoms, σ_{ij} is the distance at which the LJ has its minimum energy, ε represent the binding energy in the LJ, $\varepsilon_1 = \varepsilon\varepsilon_0$ is the effective dielectric constant and q_i and q_j are the partial atomic charges of atoms i and j. The *pair style lj/charmm/coul/charmm* was used with inner and outer cut-offs 8.0 Å and 10.0 Å, respectively which represents (3) was used for calculating non-bonded interactions of epoxy and C60 molecules. The equilibrium spacing parameters of the LJ potential (σ) were taken to be the arithmetic mean of the individual parameters of the respective atom types while the good depth parameter (ε) was taken to be the geometric mean of the values. The parameters used for the non-bonded and bonded interactions for C60 are listed in Table S3.

The *bond style morse* of the LAMMPS code was selected for calculating the bond interaction for the C60, which represents the following expression.

$$E = D\left[1\text{-}e^{-\alpha(r\text{-}r_o)}\right]^2 \quad (4)$$

where r_0 is the equilibrium bond distance, α is a stiffness parameter, and D determines the depth of the potential well.

For the angle interactions of the C60, *angle style cosine/squared* of the LAMMPS code was used, which represents the following expression.

$$E = K\,[cos\theta - cos\theta_o]^2 \quad (5)$$

where θ_0 is the equilibrium value of the angle, and K is a prefactor and note that the usual 1/2 factor is included in K.

For the dihedral interactions of the C60, dihedral_style harmonic of the LAMMPS code was used, which represents the following expression.

$$E = K\,[1 + dcos(n\varphi)] \quad (6)$$

where, K represents energy, d is a variable having value either $+1$ or -1 and n is an integer $\geqq 0$.

2.2 Preparation of the initial simulation boxes

The DGEBA and DETA monomers were randomly packed in a stoichiometric ratio of 5:2, respectively, using Packmol [34,35] software in a 46 Å cube which is comfortably larger than the lower limit imposed by the Minimum Image Convention. For the initial density of the box to be 0.5 g·cm^{-3}, 80 DGEBA and 32 DETA monomers were packed in the simulation box. The simulation box with fullerene (C60) reinforcement having a single fullerene molecule was prepared similarly and had the same number of DGEBA and DETA monomers with dimensions as that of the neat Epoxy simulation box. This resulting system had 2.3 wt% of C60. Figure 2(a) and Figure 2(b) show the simulation box containing the neat epoxy system and epoxy/C60 system, respectively. The neat epoxy system contains 4400 atoms connected by 4608 bonds, 8320 angles, 11168 dihedrals, and 800 impropers. Topotools plugin of the VMD [36] software was used to generate the topology information. LAMMPS data file containing the simulation box was then generated using the same plugin of the VMD software.

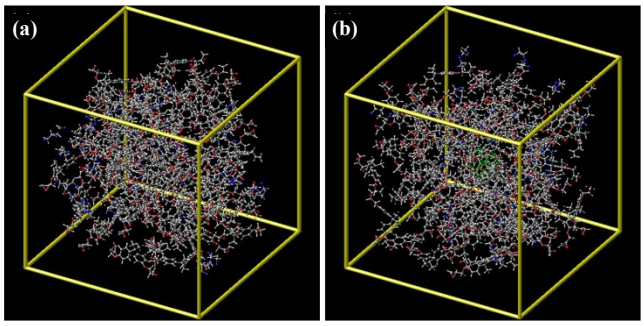

Figure 2. Simulation box containing the (a) pure epoxy system, and (b) epoxy/C60 system (C60-green color bonds at the center).

2.3 Crosslinking procedure

All the subsequent simulations were done using the LAMMPS code [37] released on 30th Oct 2014 in fourteen Intel Ivy Bridge processors in the NITS Supercomputing Center. The simulation time for the crosslinking process was about 4 ns for each system, and the cooling down process was about 40 ns, and that for the testing process was about two numbers for each crosslinking density. The total time for two systems with four crosslinking densities was about 680 ns, which took 561 CPU hours. The inner and outer cut-off ($r_{cut\text{-}off}$) for the 12-6 Lennard-Jones and the short-range electrostatics was set to 8 Å and 11 Å, respectively.

2.3.1 Equilibration

The simulation box containing the un-crosslinked mixture was first minimized and subsequently equilibrated by 50 ps NVT at 600 K and then 400 ps NPT at 1 atm and 600 K to minimize internal forces (thus reducing internal residual stresses) resulting from the construction of bonds, bond angles, and bond dihedrals. The NVT and NPT ensembles made use of the Nose/Hoover thermostat and barostat for temperature and pressure control with damping values of 100 fs and 350 fs, respectively [38]. The equilibration and subsequent simulations were performed in periodic boundary conditions.

2.3.2 Formation of C−N bonds

The Monte-Carlo package of the LAMMPS code was used for creating and breaking bonds. A threshold crosslinking cut-off (r_{crslnk}) can be selected in the Monte-Carlo package of the LAMMPS within which if two un-reacted C and N atoms lie will be bonded. In the current work, the crosslinking density, conversion degree, or percentage conversion (c) is defined as the ratio between the number of C-N bonds created and the maximum C-N bonds possible to create. The crosslinking process was initiated by setting the percentage conversion, c to 0, and r_{crslnk} to 2.64 Å followed by possible bond formation. Then the instantaneous number (i) of bonds formed was checked and for non-zero values of i, the created bonds were brought to their equilibrium bond length with a multistep minimization. The system was then subjected to 50 ps NPT at 600 K to let it relax and equilibrate to its new topology and then again, possible bonds were allowed to form. This was repeated until no more bonds can form on that crosslinking cut-off (r_{crslnk}) or i became zero. Then the crank was increased by 1 Å and the process was repeated for the new crosslinking cut-off until $r_{crslnk} > r_{cut\text{-}off}$ (11 Å) or the system becomes fully crosslinked. The state of the simulation was saved after every 50 ps NPT step for further analysis.

2.3.3 Breaking of N−H and C−O bonds and formation of O−H bonds

The C−O bonds of the reactive epoxy carbons, which bonded with N present in the hardener, must be broken to get the actual molecular topology of the crosslinked structure. So, the list of the reacted C atoms and the O atoms were used to group them, and all bonds in that group were deleted using the *delete_bonds* command. The H atoms in the amine groups must be de-bonded from the reacted N atoms and must be bonded to the O atoms of the reacted epoxy molecule. These N−H bonds were broken in the same manner as that of C−O bonds. For bonding the H atom from amine with the O atom from epoxy, the list of H and O atoms was used and was carried out using the *fix bond/create* command. Figure 3(a) and Figure3(b) show the simulation box containing the 55% crosslinked structures of the neat epoxy system and the Epoxy/C60 system, respectively.

2.3.4 Charge update

It was found that change in partial charges, topology, and parameters during the crosslinking process occurs only in the reactive ends of the monomers. The change in partial charges in DGEBA monomer, DETA monomer, and reacted DGEBA/DETA molecule is shown in Figure 4(a-c) respectively. An aspect that has not been fully explored in the crosslinking simulations is the evolution of partial atomic charges during curing. Electrostatic interactions play an important role in the overall binding of these systems and an accurate calculation of the charge distribution is essential to predict their structure and properties. In most classical molecular dynamics simulations, static atomic charges are used. However, during polymerization/crosslinking simulations, the charge distribution is expected to change when chemical reactions occur [39]. Thus, an accurate simulation of the crosslinking process should include a procedure for updating charges to take into account the changes in chemistry and topology. The list of atom IDs was used to assign charges to those atoms using the *set* command of the LAMMPS code.

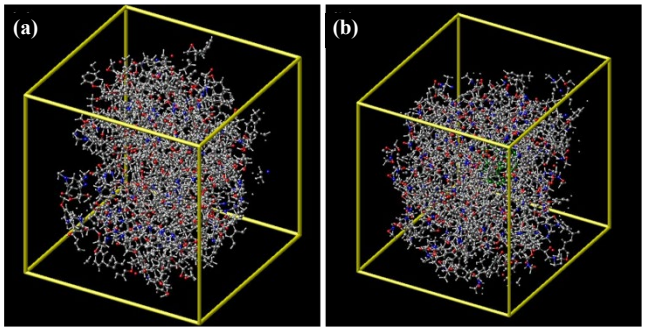

Figure 3. Simulation box containing the 55% crosslinked structure of (a) pure epoxy system and (b) epoxy/C60 system.

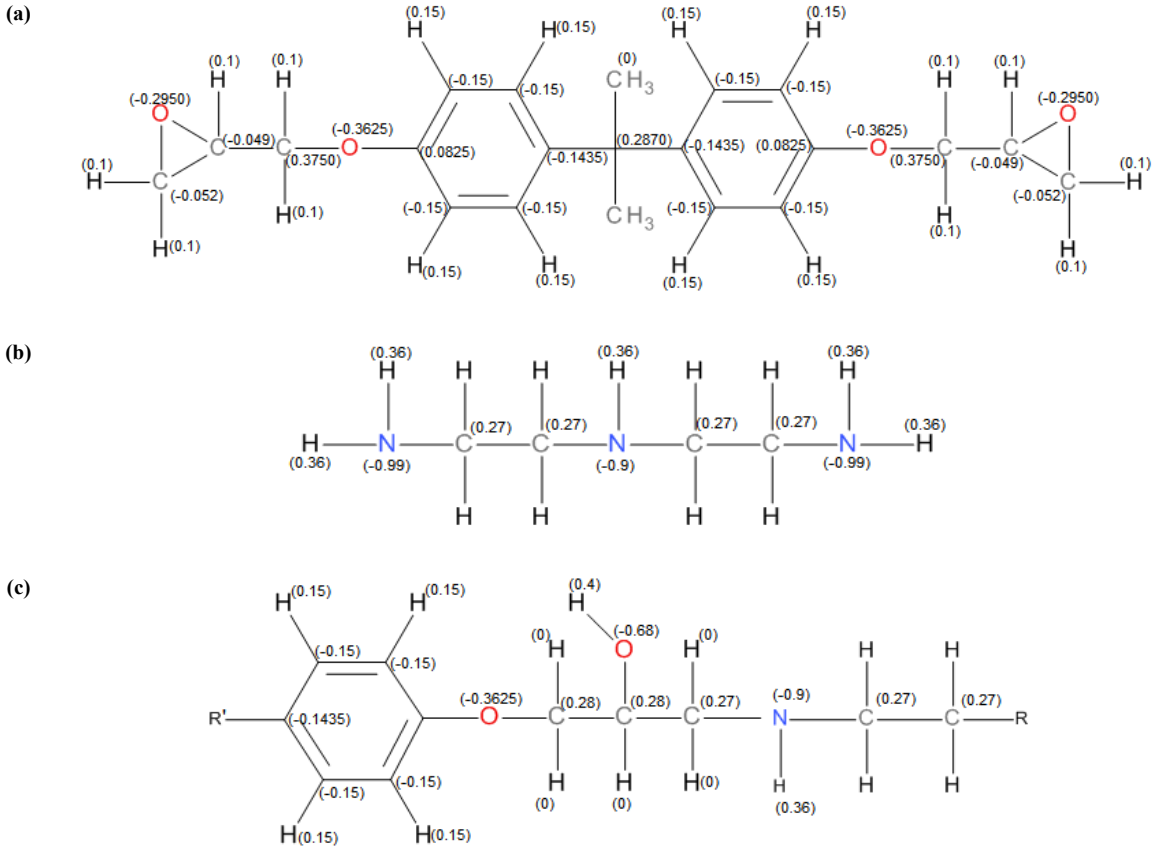

Figure 4. Partial charges of (a) DGEBA monomer, (b) DETA monomer, and (c) reacted DGEBA and DETA molecule.

2.3.5 Multi-step minimization

When a new bond is formed between a pair of reactive atoms, their separation distance is significantly larger than the equilibrium bond length. Thus, to avoid large interatomic forces between the newly connected atoms, a multistep relaxation procedure was used [39] where created bonds are brought to their equilibrium bond length in five incremental steps.

The created bonds are assigned equilibrium bond length equal to the mean of the crosslinking cut-off and the actual equilibrium bond length in five steps, as shown in Table S4. The force constant assigned was one-fifth of the regular value for the first step, two-fifths for the second step, and so on. Varshney *et al* [39] used a different bond type for each new bond; this approach leads to even smaller disruptions of the dynamics during bond creation as compared with a three-group method suggested by Li *et al* [40] which was computationally simple and scalable. The approach suggested in this paper applies to incremental crosslinking cut-off only. The method is scalable and much simpler than Varshney *et al* [39].

2.4 Simulated annealing

After the topology update, the crosslinked structure was cooled from 600 K to 300 K in the NPT thermostat at a rate of 15 K per 2 ns. The density data in the second half of every 2 ns was extracted at every 1 ps and was averaged to get the density corresponding to that temperature. The specific volume versus temperature graph was then generated for obtaining the GTT. The first two data points were neglected to eliminate the effects of molecular relaxation and initial oscillation of the temperature and pressure around the set values. Using the next eight data points, a linear regression fit was done and hence a line fitted to the corresponding data points was obtained. Similarly, using the last eight data points, a linear fit was obtained. Then the vertical line was drawn from the intersection of both the fitted lines to the temperature axis. The use of discontinuity in the slope of the density or specific volume vs. temperature graph to determine the GTT has been widely used by the researchers [39,41,42]. Hence, the linear regression fits were used at the endpoints of the specific volume versus temperature curves and the intersection of the fitted lines was noted as the GTT.

2.5 Thermal expansion coefficients

The volumetric thermal expansion coefficient was obtained using the density versus temperature data. The specific volumes at different temperatures were obtained from the density data and then the volumetric and linear thermal expansion coefficients were calculated for the system before and after the GTT using the following formulae

$$\alpha = \frac{1}{V}\left(\frac{\delta V}{\delta T}\right)_P \quad (7)$$

$$\beta = \frac{1}{3}\alpha \quad (8)$$

2.6 Elastic constants

The annealed crosslinked structure at 300 K was subjected to uniaxial tensile tests using non-equilibrium molecular dynamics, as reported by Clancy *et al* [43]. The temperature of the system was maintained using an NVT ensemble. An affine deformation was applied to the structure along a single axis at an engineering strain rate of 108 s^{-1} while keeping the deformation along the other axes fixed. Similarly, three shear deformations in the different axes were also applied to the simulation boxes. Such high strain rate loadings are usually not applied in tensile test experiments, but, they can be very useful for analyzing impact behavior. The first element of the stiffness matrix is the slope of the elastic region of the σ_{xx}versus ε_{xx}curve obtained from deformation along the x-direct. The second element of the first row is obtained similarly from the same simulation but the σ_{yx} versus ε_{xx} curve. The second and third rows were obtained from deformations along the other two axes. The elements C_{44}, C_{55}, and $Cion_{66}$, were obtained from the shear deformations. The lames constants μ and λ were obtained using the following equations.

$$\mu = \frac{4a - 2b + 3c}{33} \quad (9)$$

$$\lambda = \frac{2a + c - 15\mu}{6} \quad (10)$$

$$a = C_{11} + C_{22} + C_{33} \quad (11)$$

$$b = C_{12} + C_{13} + C_{21} + C_{23} + C_{31} + C_{32} \quad (12)$$

$$c = C_{44} + C_{55} + C_{66} \quad (13)$$

The Young's modulus, Y, was then calculated using equation (14).

$$Y = \mu\frac{3\lambda + 2\mu}{\lambda + \mu} \quad (14)$$

3. Results and discussion

3.1 Crosslinking comparison

The Figure 5(a) shows the evolution of percentage conversion with increasing crosslinking cut-off. Both the systems followed the similar trend in terms of percentage conversion with increasing crosslinking cutoff. Figure 5(b) shows an increase in the percentage of primary and secondary reactions with the increase in crosslinking cut-off. Comparing the conversions of primary and secondary amines of both the systems, it was found that more primary conversion occurred in the neat epoxy system than the secondary conversion. Figure 6(a) and Figure 6(b) shows the evolution of percentage conversion of primary amine, secondary amine, and total conversion with time for the neat epoxy system and the composite system, respectively. In the epoxy/C60 system, the secondary reaction was predominant compared to the primary reaction.

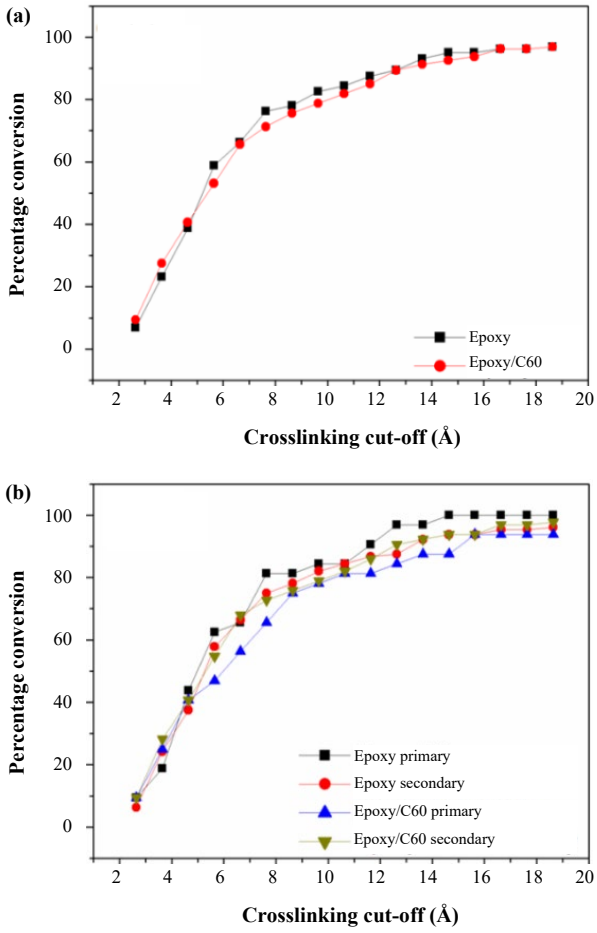

Figure 5. (a) Percentage conversion or crosslinking density vs. crosslinking cut-off for the neat epoxy and the Epoxy/C60 system, and (b) percentage conversion of primary and secondary amine vs. crosslinking cut-off for the pure and the composite system.

3.2 Volumetric properties

The volumetric properties were obtained by cooling the systems from 600 K to 300 K. The densities obtained at the end of the cooling processes were plotted for different crosslinking densities, as shown in Figure 7. It was observed that the density of the composite system is lower than that of the neat epoxy system. At lower crosslinking densities, the density of the neat epoxy system increases with an increase in cross-linking density. It reaches a maximum value of 1.10 $g{\cdot}cm^{-3}$ at a crosslinking density of 66.25%. Unlike the neat epoxy system, the density of the epoxy/C60 system remained almost constant, with a slight decrease with increasing crosslinking density. But at higher crosslinking densities, the density of the epoxy/C60 system showed an increase up to a value of 1.04 $g{\cdot}cm^{-3}$, although it was still lower than that of the maximum density value of the neat epoxy system. The epoxy/C60 system showed a lower density than that of the neat epoxy system because C60 itself has a lower density and hence it decreases the density of the composite. At higher crosslinking densities, however, the density of the epoxy/C60 system increased because the effect of more bonds created surpluses the effect of C60 lowering the density of the composite.

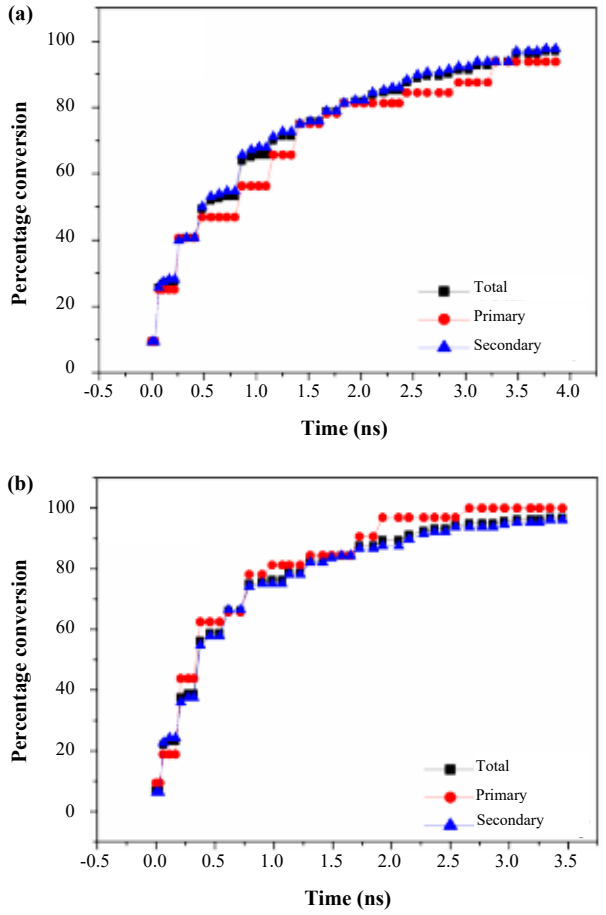

Figure 6. Total, primary, and secondary percentage conversions vs. time for the (a) pure epoxy system, and (b) epoxy/C60 system.

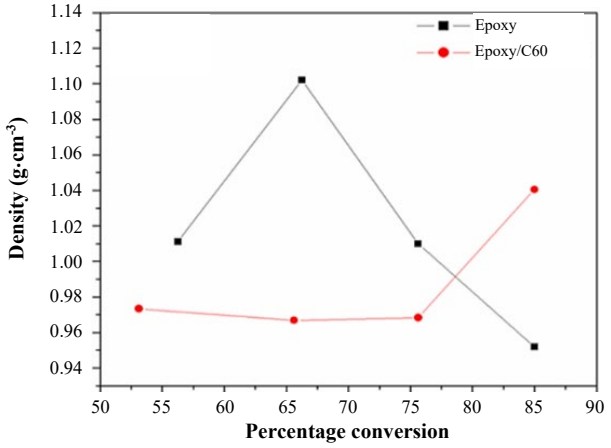

Figure 7. The densities for different crosslinking densities for the pure and composite system.

3.2.1 Glass transition temperature

The method used for obtaining the GTT from volumetric data is already mentioned in section 2.4. Figure 8(a) and Figure 8(b), which are for 55% crosslinked structure for the neat epoxy and the epoxy/C60 system respectively, are shown as examples of such plots. Figure 9 shows the variation of GTT with crosslinking density. As expected, higher crosslinking density shows higher GTT. It was also observed that the presence of C60 enhances the GTT of epoxy. The increase in GTT with crosslinking density is because, with the increase in crosslinking, there is a decrease in the number of ways the polymer chain can slide past each other and hence requiring more energy for flow to occur. Again, the higher GTT in the epoxy/C60 system may be due to the same reason if the C60 molecule hinders the movement of chains.

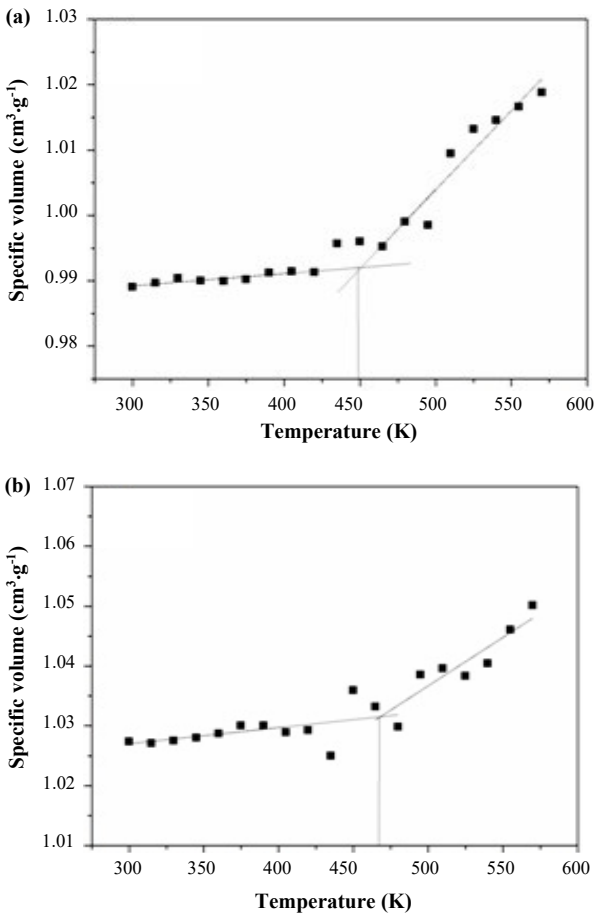

Figure 8. Specific volume versus temperature plot with regression fits for the 55% crosslinked structure of the (a) pure epoxy system and (b) C60/epoxy system.

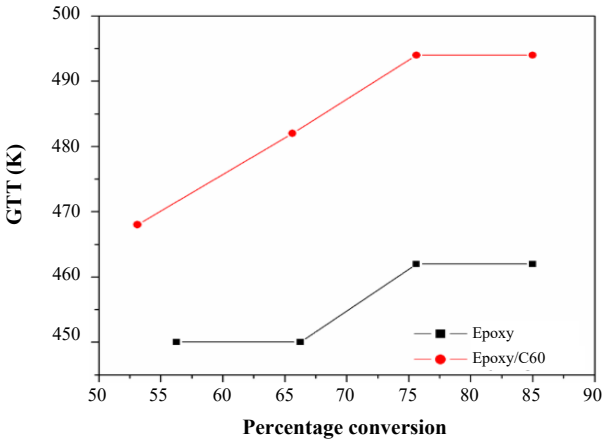

Figure 9. Glass-transition temperatures for different crosslinking densities for both the systems.

3.2.2 Coefficients of thermal expansions

The coefficients of volumetric thermal expansions (CVTE) below and above GTT were obtained from the slopes of the linear regression fits using (7). Figure 10(a) shows the variation of CVTE for below GTT for both the neat epoxy and epoxy/C60 system and Figure 10(b) shows the same for above the GTT. The CVTE below GTT of the epoxy/C60 system was found to be almost equal but slightly more than that of the neat epoxy system. Below GTT, an overall decrease in the CVTE with an increase in crosslinking density was observed for both the systems, but the Epoxy/C60 system showed an increase in the CVTE (below GTT) at higher crosslinking densities. The overall decrease is observed because at denser crosslinking, atomic vibrations are restricted. Hence the average distance separating the atoms tends to increase less with increasing temperature. As we know, volume expansion is a direct function of the average distance separating the atoms. So, the CVTE below GTT, which is a measure of volume expansion due to increasing temperature, decreases with increasing temperature.

Above the GTT, the material is not in solid-state, rather it is in a soft and rubbery state. The volumetric behaviour above GTT is, therefore, completely different than that below GTT, although it shows the same overall trend of decreasing with increasing crosslinking density. The reason for the overall decreasing trend may be the same as the one for below GTT as the laws of solid-state physics holds even in the rubbery state. Unlike the case below GTT, the CVTE above GTT is mainly lower for the epoxy/C60 system than that of the neat epoxy system. This may be due to the rubbery nature of the epoxy, which causes the epoxy to expand into spaces created between C60 molecules, which was not possible below GTT. If the plot of CVTE above GTT vs. crosslinking density is closely observed, it can be seen that for the epoxy/C60 system, the CVTE above GTT first increases, then decreases and again increases with increasing crosslinking density. But for the neat epoxy system, the CVTE above GTT first shows a decrease then shows the increase, and then again shows a decrease in value. The coefficients of linear thermal expansions can be obtained from the coefficients of volumetric thermal expansions using equation (5).

3.3 Young's modulus

As mentioned in section 2.6, uniaxial tensile simulations were performed using non-equilibrium molecular dynamics to find the coefficients of the stiffness matrix. Figure 11 shows the variation of Young's modulus with crosslinking density for both the neat and composite systems. The results show an increase in Young's modulus with an increase in cross-linking density. Also, Young's modulus was lower for the epoxy/C60 system compared to the neat one. At lower and medium crosslinking densities, the young's modulus for the epoxy/C60 system was higher than that of the neat epoxy system. This is because the fullerene restricts the mobility and deformation of the matrix by introducing a mechanical restraint. Since Young's modulus directly varies with restriction in polymer chain mobility, Young's modulus was higher for the Epoxy/C60 system than that of the neat epoxy system. It was observed that for the neat epoxy system, the Young's modulus steadily increases with an increase in cross-linking density. This behavior can be attributed to more number of crosslinking bonds in higher crosslinking density, which increases the stiffness of the material. For the epoxy/C60 system, the Young's modulus first increases for lower crosslinking densities and then decreases for moderate and higher crosslinking densities. The initial increase is due to an increase in the number of crosslinking bonds, which leads to an increase in the stiffness of the material.

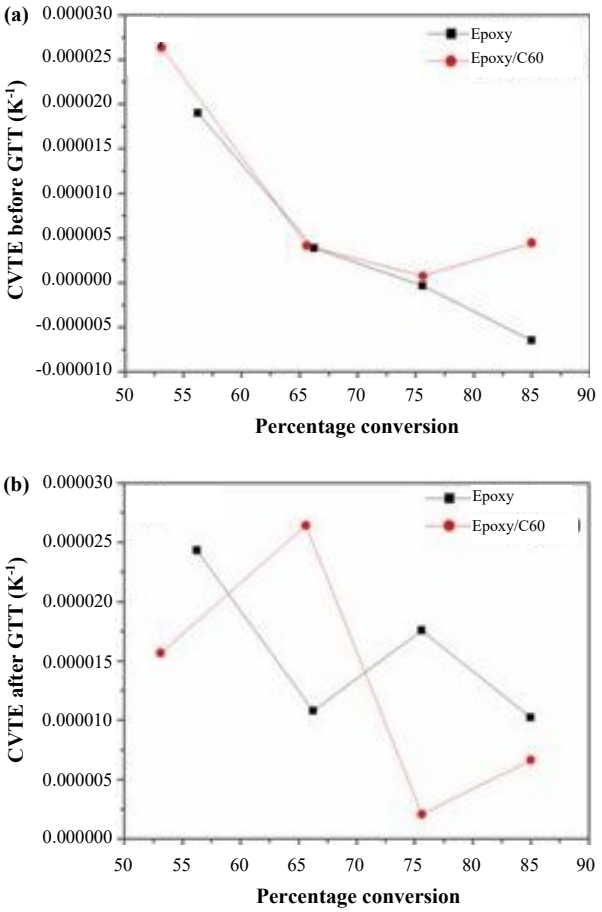

Figure 10. Variation of coefficient of volumetric thermal expansion with crosslinking density (a) below GTT and (b) above GTT.

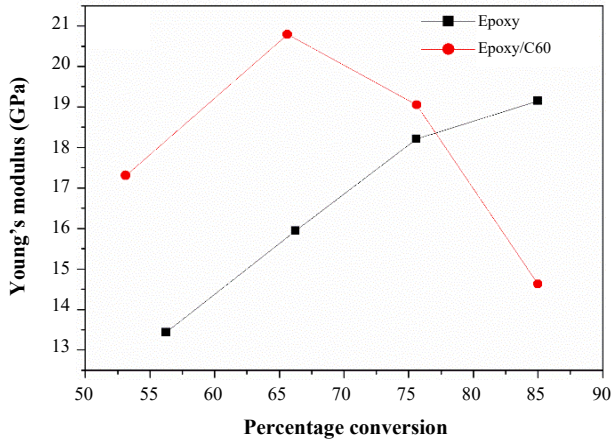

Figure 11. Variation of Young's modulus with crosslinking density.

Table 1. Young's modulus and glass transition temperatures of epoxy/C60 composites.

C60 (wt%)	Matrix system	Increase % in Young's modulus	Increase % in glass transition temperature	Ref.
1.0 (Theoretical)	phenol novolak resin + cycloaliphatic diamine	20 %	1.2 %	[16]
10 (Theoretical)	cis-1,4-poly(butadiene)	---	1.7%	[17]
1.0 (Experimental)	DGEBA + ---	21.5 %	---	[44]
0.5 (Experimental)	DGEBA + TETA	---	-8.75%	[7]
0.5 (Experimental)	DGEBA + TETA	16.5 %	---	[8]
2.3 (Theoretical)	DGEBA/DETA	-23.7%	6.9%	Current work

However, the comparison of both Young's modulus and glass transition temperature of epoxy/C60 composite indicate huge variation that may be due to the use of different monomers of epoxy as well as C60 content compared to other studies. However, the increased glass transition temperature shows an increment which is following similar trend as reported by the others, but the decline in Young's modulus is unexpected which needs to be optimized further.

For comparison of obtained results, a verification is performed on the simulation results. Both the theoretical and experimental results of Young's modulus and glass transition temperature of epoxy/C60 composite are displayed in Table 1.

4. Conclusions

In the current study, MD simulations were performed on atomistic models of neat epoxy and epoxy/C60 systems to probe into the effect of introducing a C60 in physical, thermo-physical, and mechanical properties in cross-linked polymers. The crosslinked epoxy system was generated using MD, Multistep Minimization, and Monte Carlo bond-forming and breaking techniques. The changes in partial atomic charges were taken care of by the electrostatic equilibration-based charge assignment method. *GTT* of epoxy was observed to be increased by about 25°K due to the introduction of C60. The increase in GTT with increasing crosslinking density was higher in case of the composite compared to the neat epoxy. The presence of C60 increased the density of the composite at higher crosslinking densities of epoxy. The coefficients of thermal expansion (CTE) decreased with increasing crosslinking density for both the epoxy and the epoxy/C60 system. The presence of C60 hardly affected the CTE of the epoxy. The Young's modulus of the epoxy/C60 system decreased compared to neat epoxy system.

Supporting information

We have given DFT optimized geometrical parameters of DGEBA and DETA in Table S1 and Table S2 respectively. Table S3 gives parameters for atomic interactions of C60 and Table S4 lists equilibrium bond length and Force constant assigned to created bonds at given steps. We also provide detail of the atom list of generation in Text S1.

Acknowledgement

AKM acknowledges UPES SEED grant (year 2021) for computing facilities.

References

[1] B. Ellis, Chemistry and Technology of Epoxy resins, 1993. doi:10.1007/978-94-011-2932-9.

[2] F. L. Jin, X. Li, and S.J. Park, "Synthesis and application of epoxy resins: A review," *Journal of Industrial and Engineering Chemistry*, vol. 29, pp. 1-11, 2015.

[3] A. Shokuhfar, and B. Arab, "The effect of cross linking density on the mechanical properties and structure of the epoxy polymers: Molecular dynamics simulation," *Journal of Molecular Modeling*, vol. 19, pp. 3719-3731, 2013.

[4] B. Qi, Q. X. Zhang, M. Bannister, and Y. W. Mai, "Investigation of the mechanical properties of DGEBA-based epoxy resin with nanoclay additives," *Composite Structures*, vol. 75, pp. 514-519, 2006.

[5] S. K. S., and I. Jena, "Polymer/carbon nanotube nano-composites: A novel material," *Asian Journal of Chemistry*, vol. 22, pp. 1-15, 2010.

[6] M. Loos, Chapter 6 - Processing of polymer matrix composites containing CNTs, 2015.

[7] S. Das, S. Halder, and K. Kumar, "A comprehensive study on step-wise surface modification of C60: Effect of oxidation and silanization on dynamic mechanical and thermal stability of epoxy nanocomposite," *Material Chemistry and Physics, vol.* 179, pp.120-128, 2016.

[8] S. Das, S. Halder, A. Sinha, M. A. Imam, and N. I. Khan, "Assessing nanoscratch behavior of epoxy nanocomposite toughened with silanized fullerene," *ACS Applied Nano Materials*, vol.1, pp. 3653-3662, 2018.

[9] P. Lin, and R. Khare, "Molecular simulation of cross-linked epoxy and epoxy - POSS nanocomposite," *Macromolecules*, vol. 42, pp. 4319-4327, 2009.

[10] B. J. Alder, and T. E. Wainwright, "Phase transition for a hard sphere system," *Journal of Chemical Physics*, vol. 27, pp. 1208-1209, 1957.

[11] S. J. V. Frankland, V. M. Harik, G. M. Odegard, D. W. Brenner, and T. S. Gates, The stress – strain behavior of polymer – nanotube composites from molecular dynamics simulation," *Composites Science and Technology*, vol. 63, pp. 1655-1661, 2003.

[12] R. Rahman, J. T. Foster, and A. Haque, "Molecular dynamics simulation and characterization of graphene-cellulose nano-composites," *Journal of Physical Chemistry A*. vol.117, pp. 5344-5353, 2013.

[13] K. S. Khare, and R. Khare, "Effect of carbon nanotube dispersion on glass transition in cross-linked epoxy-carbon nanotube nanocomposites: Role of interfacial interactions," *Journal of Physical Chemistry B*, vol. 117, pp. 7444-7454, 2013.

[14] C. Jiang, J. Zhang, S. Lin, and D. Jiang, "Molecular dynamic simulation study on glass transition temperature of DGEBA-THPA / SWCNTs composites," *Journal of Materials Science and Chemical Engineering*, vol. 2, pp. 26-30, 2014.

[15] A. Adnan, C. T. Sun, and H. Mahfuz, "A molecular dynamics simulation study to investigate the effect of filler size on elastic properties of polymer nanocomposites," *Composites Science and Technology*, vol. 67, pp. 348-356, 2007.

[16] S. F. Ferdous, M. F. Sarker, and A. Adnan, "Role of nanoparticle dispersion and filler-matrix interface on the matrix dominated failure of rigid C60-PE nanocomposites: A molecular dynamics simulation study," *Polymer*, vol. 54, pp. 2565-2576, 2013.

[17] F. Jeyranpour, G. Alahyarizadeh, and A. Minuchehr, "The thermo-mechanical properties estimation of fullerene-reinforced resin epoxy composites by molecular dynamics simulation - A comparative study," *Polymer (Guildf)*, vol. 88, pp. 9-18, 2016.

[18] Y. Y. Gao, F. Y. Hu, J. Liu, and Z. Wang, "Molecular dynamics simulation of the glass transition temperature of fullerene filled cis-1,4-polybutadiene nanocomposites," *Chinese Journal of Polymer Science,* vol. 36, pp. 119-128, 2018.

[19] C. S. Ezquerro, M. Laspalas, A. Chiminelli, F. Serrano, and C. Valero, "Interface characterization of Epoxy resin nanocomposites: A molecular dynamics approach," *Fibers*, vol. 6, p. 55, 2018.

[20] K. Fu, Q. Xie, F. Lü, Q. Duan, X. Wang, Q. Zhu, and Z. Huang, "Molecular dynamics simulation and experimental studies on the thermomechanical properties of epoxy resin with different anhydride curing agents," *Polymers,* vol. 11, pp. 1-15, 2019.

[21] A. Yadav, A. Kumar, P. K. Singh, and K. Sharma, "Glass transition temperature of functionalized graphene epoxy composites using molecular dynamics simulation," *Integrated Ferroelectrics*, vol. 186, pp. 106-114, 2018.

[22] M. J. Frisch, G. W. Trucks, H. B. Schlegel, et al. Gaussian, Inc., Wallingford CT, 2016.

[23] A. Frisch, A. B. Nielson, and A. J. Holder, GAUSSVIEW User Manual, Gaussian Inc., Pittsburgh, PA, USA, 2000.

[24] A. D. Becke, "Density-functional exchange-energy approximation with correct asymptotic behaviour," *Physical Review A*, vol. 38, pp. 3098-3100, 1988.

[25] R. G. Parr, and W. Yang, "Density functional theory of atoms and molecules," Oxford University Press: New York, 1989.

[26] C. Lee, W. Yang, and R. G. Parr, "Development of the Colle-Salvetti correlation-energy formula into a functional of the electron density," *Physical Review B*, vol. 37, pp. 785-789, 1998.

[27] A. D. Becke, "Density-functional thermochemistry. III. The role of exact exchange," *Journal of Chemical Physics*, vol. 98, pp. 5648-5652, 1993.

[28] A. Pizzi, and K. L. Mittal, "Handbook of adhesive technology, revised and expanded," CRC Press, 2003.

[29] M. D. Hanwell, D. E. Curtis, D. C. Lonie, T. Vandermeersch, E. Zurek, and G. R. Hutchison, Avogadro : an advanced semantic chemical editor, visualization , and analysis platform, pp. 1-17, 2012.

[30] Avogadro: An open-source molecular builder and visualization tool. Version 1. XX. http://avogadro.cc/.

[31] B. R. Brooks, C. L. Brooks, A. D. Mackerell, L. Nilsson, R. J. Petrella, B. Roux, Y. Won, G. Archontis, C. Bartels, S. Boresch, A. Caflisch, L. Caves, Q. Cui, A. R. Dinner, M. Feig, S. Fischer, J. Gao, M. Hodoscek, W. Im, K. Kuczera, T. Lazaridis, J. Ma, V. Ovchinnikov, E. Paci, R. W. Pastor, C. B. Post, J. Z. Pu, M. Schaefer, B. Tidor, R. M. Venable, H. L. Woodcock, X. Wu, W. Yang, D. M. York, and M. Karplus, "CHARMM: the biomolecular simulation program.", Journal of Computational Chemistry, vol. 30, pp. 1545-614, 2009.

[32] V. Zoete, M. A. Cuendet, A. Grosddier, and O. Michielin "SwissParam : A fast force field generation tool for small organic molecules," *Journal of Computational Chemistry* vol. 32, pp. 2359-2368, 2011.

[33] F. A. Momany, and R. Rone, "Validation of the general purpose QUANTA ®3.2/CHARMm® force field," *Journal of Computational Chemistry,* vol. 13, pp. 888-900, 1992.

[34] K. Vanommeslaeghe, E. Hatcher, C. Acharya, S. Kundu, S. Zhong, J. Shim, E. Darian, O. Guvench, P. Lopes, I. Vorobyov, and A. D. Mackerell, "CHARMM general force field: A force field for drug-like molecules compatible with the CHARMM all-atom additive biological force fields," *Journal of Computational Chemistry*, vol. 31, pp. 671-90, 2010.

[35] W. Yu, X. He, K. Vanommeslaeghe, and A. D. MacKerell, "Extension of the CHARMM General Force Field to sulfonyl-containing compounds and its utility in biomolecular simulations," *Journal of Computational Chemistry*, vol. 33, pp. 2451-2468, 2012.

[36] L. Martínez, R. Andrade, E. G. Birgin, J. M. Martínez, "PACKMOL: A package for building initial configurations for molecular dynamics simulations," *Journal of Computational Chemistry,* vol. 30, pp. 2157-2164, 2009.

[37] M. Marti, and L. Marti, "Packing optimization for automated generation of complex system's initial configurations for molecular dynamics and docking," *Journal of Computational Chemistry*, vol. 24, pp. 819-825, 2003.

[38] W. Humphrey, A. Dalke, and K. Schulten, "VMD - Visual molecular dynamics", *Journal of Molecular Graphics*, vol. 14, pp. 33-38, 1996.

[39] S. Plimpton, "Fast parallel algorithms for short – Range molecular dynamics," *Journal of Computational Physics,* vol. 117, pp.1-42, 1995.

[40] G. J. Martyna, D. J. Tobias, and M. L. Klein, "Constant pressure molecular dynamics algorithms". *Journal of Chemical Physics.* vol. 101, pp. 4177-4189, 1994.

[41] M. Parrinello, "Polymorphic transitions in single crystals: A new molecular dynamics method", *Journal of Applied Physics*, vol. 52, p. 7182, 1981.

[42] M. E. Tuckerman, J. Alejandre, R. López-Rendón, A. L. Jochim, and G. J. Martyna, "A Liouville-operator derived measure-preserving integrator for molecular dynamics simulations in the isothermal–isobaric ensemble," *Journal of Physical A. Math. Gen.*, vol. 39, pp. 5629-5651, 2006.

[43] W. Shinoda, M. Shiga, M. Mikami, and M. Carlo, "Rapid estimation of elastic constants by molecular dynamics simulation under constant stress," *Physical Review B*, vol. 69, pp. 16-18, 2004.

[44] V. Varshney, S. S. Patnaik, A. K. Roy, and B.L. Farmer, "A molecular dynamics study of epoxy-based networks: Cross-linking procedure and prediction of molecular and material properties," *Macromolecules,* vol. 41, pp. 6837-6842, 2008.

[45] C. Li, and A. Strachan, "Molecular scale simulations on thermoset polymers: A review," *Journal of Polymer Science Part B Physics*, vol. 53, pp. 103-122, 2011.

[46] A. Bandyopadhyay, P. K. Valavala, T. C. Clancy, K. E. Wise, and G. M. Odegard, "Molecular modeling of crosslinked epoxy polymers : The effect of crosslink density on thermomechanical properties," *Polymer (Guildf),* vol. 52, pp. 2445-2452, 2011.

[47] J. L. Tack, and D. M. Ford, "Thermodynamic and mechanical properties of epoxy resin DGEBF crosslinked with DETDA by molecular dynamics," *Journal of Molecular Graphics and Modelling*, vol. 26, pp. 1269-1275, 2008.

[48] T. C. Clancy, and J. A. Hinkley, Coarse-grained and atomistic modeling of polyimides, NASA/TM-213030, 2004.